Geometric Optimization for a Complex Supersonic Rectangular Nozzle

Tyler M. Vartabedian
Department of Mechanical and Aerospace Engineering
Syracuse University
Syracuse, NY 13244, USA
tmvartab@syr.edu

***Abstract*—A method for geometric optimization of an aft-deck plate of a complex, supersonic jet nozzle is presented. A combination of data fusion, experiments, and machine learning techniques are utilized. The presented algorithm employs a genetic algorithm in tandem with an artificial neural network. This simultaneously predicts far-field overall sound pressure levels while searching for optimal coordinates of the aft-deck plate body points. The parameters of the genetic algorithm restrict the resulting points to realistic positions in a 2D plane. The generated deck plate geometries are experimentally tested to verify acoustic spectra predictions while continuing to train the artificial neural network. Results indicate an accurate incorporation of the genetic algorithm into the artificial neural network while providing a slight reduction in overall sound pressure levels.**

***Index Terms*—genetic algorithms, shape optimization, complex nozzle, neural networks, acoustic prediction**

I. Introduction

The aerospace industry continues to develop more advanced engines to improve aircraft capabilities and performance. The goal of flying faster and farther has been enabled by the incorporation of complex nozzles. Design alterations to these complex nozzles have utilized multiple high-velocity streams ejected through a non-axisymmetric exit. An example of a modern design featuring a Single Expansion Ramp Nozzle (SERN) in a variable cycle engine was discussed by Simmons [6] (see Fig. 1). This features a rectangular SERN with an additional bypass stream.

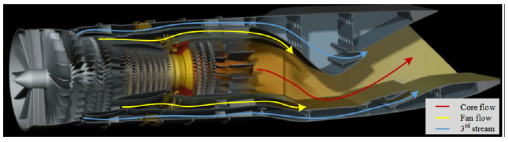

Fig. 1. Variable Cycle Engine by Simmons [6].

This configuration has been shown to allow for decreased pressure drag compared to axisymmetric nozzles, incorporated thrust vectoring, easier airframe integration, and improved off-design performance. The system includes a secondary bypass stream, referred to as the 3rd or deck stream in this study. This cool, low pressure stream protects the airframe from the hot core (combination of the fan and first bypass streams) stream while reducing noise and the resulting drag. The fundamental flow physics of this model have been explored utilizing a Multi-Aperture Rectangular SERN (MARS) (see Fig. 2).

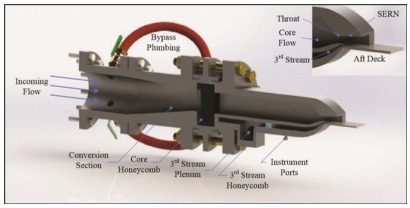

Fig. 2. Cross-Section Rendering of MARS Jet [2].

The MARS separates the two canonical flows via a splitter plate with nominal conditions of Nozzle Pressure Ratio (NPR) of 4.25 for the core flow and 1.89 for the 3rd stream (Mach 1.6 and 1, respectively). This supersonic operating condition results in a complex, turbulent environment dominated by an acoustic emission centered around 60° from the jet axis. Multiple studies [2], [3], [7], [8] have showed this instability compromises the beneficial effects of the complex system. This has been attributed to the mixing aft of the splitter plate of the two flows. This generates an incredibly complex vortex shedding instability that deflects down into the aft-deck plate boundary layer and propagates downstream. The varied-density streams, along with the supersonic nature of the nominal operating conditions, create a series of reflected shock trains and expansion waves. These complex characteristics reflect off the MARS, the aft-deck plate, and the resulting shear layers at the exit of the nozzle. Figure 3 shows the aerodynamic features as described.

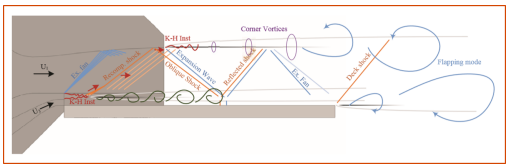

Fig. 3. MARS Shock Structure [2].

Major flow characteristics have been simulated using Large Eddy Simulations (LES) by Stack & Gaitonde [7] and experimentally verified by Berry [2], and Magstadt [3]. Gist et al [9]

expand upon these prior results while continuing to explore the aft-splitter plate region and resulting instabilities. Specifically, the splitter plate shedding was explored in depth by Stack & Gaitonde [8]. Simulations have been shown that altering this splitter plate thickness reduces the energies associated with the resulting shear instabilities [10]. The varied shear conditions were also found to impact the directionality of the far-field noise in the sideline plane [1]. Although the OASPL is dominated by a characteristic 34 kHz instability and has been heavily studied, other noise-inducing instabilities have yet to be targeted for optimization. Low-frequency components (<10,000 Hz) outside of the jet and in the far field are tied to the dynamics associated with the bulk flow [1]. These complex, reflected interactions can be impacted by the surrounding geometries of the splitter plate and the aft-deck plate. The goal of this study is to analyze these low-frequency components and reduce the associated energies through geometric optimization.

Tenney [1] applied data fusion and modern computational techniques to develop a rapid far-field overall sound pressure level (OASPL) prediction algorithm. The resulting neural network supplements the inability to collect time-resolved full-field velocity measurements. This is due to the short timescales associated with the flow from the MARS nozzle in its current configuration. This was the first application of machine learning to this system and serves as a basis for this study. Tenney's [1] artificial neural network (ANN) is expanded upon in this study to provide a rapid OASPL prediction technique in tandem with a developed genetic algorithm (GA) with the goal of designing optimized aft-deck plate geometries. The ANN predicts OASPL to within ± 4 dB utilizing simple operating parameters and geometric properties for inputs [1].

Genetic algorithms have been shown to be excellent and computationally efficient geometric optimizers. Holst & Pulliam [5] showed the ease of implementation for a GA when applied to aerodynamic shape optimization. Valackaite et al [4] found slight improvements to original geometric constraints utilizing a simple GA optimizing points in a 2D plane. GA's typically rely on population sizes in the few hundreds to few thousands to deliver reliable results. This leads to the incorporation of the ANN to supplement a lack of available (and testable) aft-deck plates. Without the use of a predictive neural network, every individual of every population would need to be manufactured and tested to analyze its fitness. Currently, 27 deck plates have been manufactured and run at a variety of conditions while probing far-field acoustic spectra. A select few of these plates were employed to train the existing ANN under varied operating conditions [1]. An example of sampled far-field acoustic spectra is shown in Fig. 4.

The purpose of this paper is to develop a 2D geometric optimization GA to work in tandem with a new NN with the goal of reducing the low-frequency noise propagating from the MARS system. The results from this investigation can be manufactured and installed into the system for further validation and improvement. Insights gained from these results could be utilized to influence next-generation aircraft fighter nozzle geometry and airframe integration.

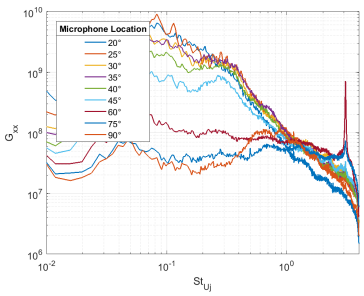

Fig. 4. Acoustic Spectra for Nominal Conditions and Nominal Aft-Deck Plate.

II. Problem and Data Description

The aerospace industry is constantly plagued by noise in both commercial and military applications. Noise is heavily prevalent in the system described prior and is primarily motivated by turbulent instabilities. Reducing the energies of these instabilities can reduce the OASPL of the system. The MARS was designed for research focused on the underlying (and relatively unknown) flow physics. No analysis was put into noise reduction, initially. Acoustic analyses and considerations are often omitted from early commercial nozzle design processes. This project aims to tackle one aspect of noise reduction: reducing the acoustic propagation of low frequency instabilities. Turbulent mixing noise is generated by the interaction of vortical structures produced by mean shear in the jet, and jet screech is produced when the upstream propagating part of the acoustic field creates a feedback loop with fluctuations originating at the nozzle lip [1]. Noise reduction will be done by geometric optimization of the MARS aft-deck plate. Preliminary experiments show a reduction in the OASPL when comparing two original deck plate geometries created by Magstadt [3] and Berry [2] (specifically a "no deck" case versus the nominal case, see Fig. 18). Modifying the aft-deck plate geometries into more complex shapes can likely yield a more ideal solution that reduces far-field noise.

An issue encountered with solving this issue comes with the lengthy data acquisition process and lack of diverse deck plate geometries. 27 deck plates are currently utilized with the MARS. Due to these two issues, a low-dimensional rapid noise prediction method is required. However, simulating acoustic emissions for complex flows is difficult and computationally expensive. Typically, Ffowcs Williams-Hawkings (FWH) surfaces are used in conjunction with CFD models to estimate far-field noise [1]. Instead of using these traditional modeling methods, can large amounts of data and artificial neural networks be leveraged to make far-field OASPL predictions? Can geometric optimization of the aft-deck plates reduce energies of the low-frequency instabilities in this system? Can a GA produce accurate results entirely dependent on using a predictive a neural network as its fitness function?

Objectives:

- Expand neural network to include more abstract data points.

- Restructure neural network to include and account for the new splitter plate geometry, new deck plate geometry inputs, and obtain corresponding training data sets experimentally.
- Maintain similar accuracy achieved by prior neural network model.
- Incorporate GA for deck plate optimization utilizing the neural network to supplement the low population, serve as the fitness function, and prevent the need to manufacture and test potentially useless deck plates.

A few data sets are considered to complete these objectives. First, the existing deck plate geometries were digitized to describe their shape using 2D-coordinates. Existing plates were previously generated utilizing three varied coordinate points mirrored about the center axis, leading to a maximum of 3 varied points (6 with symmetry). This is a limiting factor of the prior design parameters, so these coordinates were interpolated to show 76 distinct points. All outputting deck plate geometries from the GA will include 76 points.

The sampled acoustic spectra output large data sets. The 10 far-field microphones sample at 100kHz. Employed acoustic data sets were sampled in 10 second increments in a variety of flow conditions with varied deck plate geometries. This output includes 10 million distinct points for each test, 1 million from each sampled microphone. These data sets are labeled and tied to the input flow conditions and deck plate geometries. The data deployed to train the neural network for prediction is shown in 8. This is a visualization of the 290 training cases and 10 validation cases. The markers are scaled by the length of the aft deck plate length, with the smallest corresponding to the no deck case. They are also colored to represent the NTR of the core stream.

III. Approach

Modern computational methods were used in conjunction with experimental techniques. Fusing the strengths of both allows for validation of results and further training of the NN. Experimental measurements were performed to provide training data for the NN and verify its accuracy. These methods encompassed a variety of basic flow inputs with differing aft-deck plate geometries. The OASPL data was recorded, processed and fed into the NN. The existing and tested deck plate geometries were digitized as coordinates in a 2D plane to accompany the recorded acoustic data. The GA utilized all of these data sets to provide optimized aft deck geometries. The geometries can then be manufactured and installed into the MARS for experimental verification of the predicted results.

A. Experimental Methods

All experiments were performed in the Skytop Turbulence Laboratories anechoic chamber located at Syracuse University's south campus. This is a 206 m^3 acoustically treated chamber features near-field dynamic pressure transducers, a particle image velocimetry (PIV) setup, and a far-field acoustic array. The facility is fitted with 10 far-field microphones to capture acoustics at a rate of 100 kHz. The facility is shown in Figures 5 and 6.

Fig. 5. Anechoich Chamber at Skytop Turbulence Laboratories, Syracuse NY.

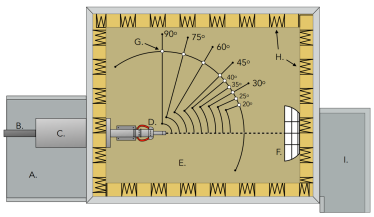

Fig. 6. Anechoic Chamber Layout: *A. Plenum Chamber, B. Jet Feed Pipe (to compressed air tanks), C. Bypass Air Flow Straightener, D. Jet Rig, E. Anechoic Chamber, F. Plume Catcher, G. Far- Field Condenser Microphones, H. Acoustic Fiberglass Wedges, I. Exhaust Path* [2].

This experimental facility allows for an easily modifiable test environment. Basic flow characteristics can be changed along with varied aft deck-plate geometries easily and quickly. Flow characteristics that were altered include the primary stream nozzle ratio (NPR_1), third stream nozzle pressure ratio (NPR_3), and the nozzle temperature ratio (NTR). Some example deck plate geometries are shown in Figure 10.

The far-field acoustic microphone array is setup in the same plane as the SERN but allows for off-plane sampling if desired. The 10 microphones are G.R.A.S. 46BE free-field condenser microphones and feature a dynamic range of 160 dB with a noise floor of 30 dB. The microphones were setup in 15°increments from 90°to 20°from the jet axis in a semi-circular arc 86.6 D_h from the nozzle exit plane. Figure 7 shows the far-field microphone array.

To train the neural network, 300 test runs were performed in 10 second sampling increments. The sampled acoustic data was post processed to calculate the OASPL. The noise model domain is shown in Figure 8 for the collected training and validation data.

B. Computational Methods

A GA and a neural network were employed for this project. The NN utilized Python with Keras as a high-level API along with Google's TensorFlow. These were chosen due to their ease of use and proven abilities. Computation was performed on an Alienware13, featuring an Intel i7 2.40 GHz processor, 16 GB of memory, and a dedicated NVIDIA GeForce GTX 860M graphics processor.

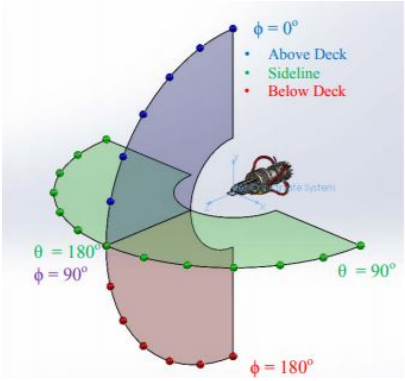

Fig. 7. Acoustic Array Layout [2].

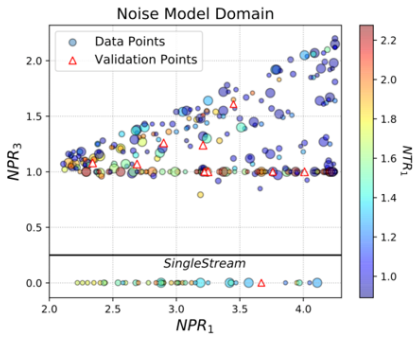

Fig. 8. Noise Model Domain [1].

1) Genetic Algorithm: The Canonical GA is used to provide the desired results of this project and all optimization methods. Canonical GA's specifically operate with selection, then crossover, then mutation. GA's operate by discretely describing the optimization space using a number of genes, x_i^n. The i-subscript corresponds to the gene number and the n-superscript shows the generation. Each individual (aft deck plate) has a set of genes that describes it, in this case the coordinates of the aft deck plate end points. The set of genes is referred to as the chromosome, given by:

$$X_j^n(x_{1,j}^n, x_{2,j}^n, ..., x_{i,j}^n, ..., x_{N,j}^n) \quad (1)$$

Where X_j^n is the jth chromosome for the nth generation of N genes. For shape optimization, bit strings are used to represent genes while the GA operators directly operate these bit strings. Real-number encoding is typically used to represent all genes. This has been shown to be more computationally efficient [5]. Specifically, y coordinates compose the chromosome, such as:

$$X = (y_1, , y_2, ..., , y_N) \quad (2)$$

Next, the initial generation is formed, represented by:

$$G^0 = (X_1^0, X_2^0, ..., X_j^0, ..., X_N^0) \quad (3)$$

Following the initial creation of the first generation, fitness functions are evaluated for each individual. The fitness function is determined by magnitude of the average OASPL. This will utilize the developed neural network for rapid prediction of the OASPL without the need for manual experimentation and data acquisition. This value was normalized.

Next, the first operation is applied, selection. This will determine which individuals will undergo the additional operations. Selection will be fitness-proportionate, often referred to as roulette-wheel selection. This selects the parents subjected to crossover, the next GA operator. This creates offspring from the selected parents to create the next generation. The offspring from one generation will also be accompanied by some particularly high fitness individuals, which is referred to as elitism.

Crossover can take multiple forms, such as single point and double point crossover. Typically the crossover selection percentage is typically high, on the order of 80%. Both single point, two point, uniform, and random average crossover will be examined and compared. For example, random average crossover is implemented by the following:

$$x_{i,j}^{n+1} = \frac{1}{2}(x_{i,j1} + x_{i,j2}) \; for \; i = 1, 2, ..N \quad (4)$$

Pairs of individuals are grouped to perform crossover. This is followed by mutation, which prevents premature convergence by maintaining genetic diversity. Here, a gene randomly changes its value with a probability p_m. Mutation magnitude values will be limited to restrict generating unrealistic individuals.

The population must remain constant so the remaining individuals are discarded. Duplicate individuals are deleted. Limits were set to individuals as well. Unrealistic individuals will be discarded. For example, a constraint on distance between two distinct points (or genes) is set to prevent an unmanufacturable deck plate. Individuals that violate this rule will be discarded. There is also a base and finite limit for y coordinates, meaning a two foot long deck plate is unrealistic and will be discarded. This process repeats for the defined generations N.

The GA settings are summarized in the following table:

Generations	100
Population Size	150
Selection	Roulette
Crossover	1PX
Mutation	2%
Elitism	Enabled

Fig. 9. Genetic Algorithm Features.

As mentioned prior, the deck plate geometries were digitized and normalized for incorporation into the genetic algorithm. An example of commonly used plates is shown in Fig 10. This includes the nominal case, no deck case, "infinite" width case, and two extended length cases, including the maximum allowed length of 233 mm.

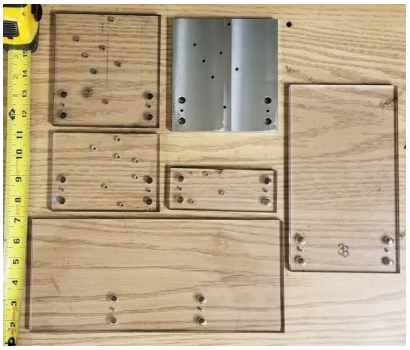

Fig. 10. Example Aft Deck Plates.

All current plate distinct coordinates points were measured by hand and recorded. See Fig. 11 for a visual example.

Fig. 11. Example Aft Deck Plate With Highlighted Coordinate Points

This figure is an example of the symmetry present with only 3 distinct coordinate points. Simpler shapes exist, such as the left of Fig. 12. Despite only having one distinct point, interpolation methods were utilized to apply multiple points to the shape for use in the GA, as seen visually on the right of 12.

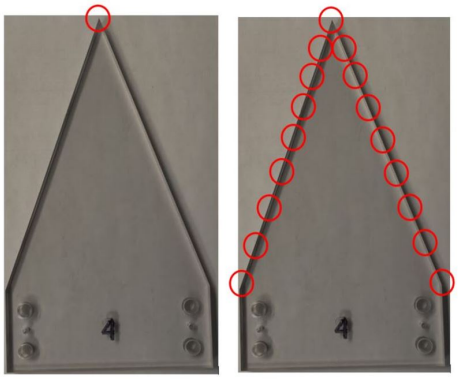

Fig. 12. Simple Aft Deck Plate Example.

A few normalization methods were utilized for the deck plate geometries. First, the x-coordinates were normalized about the width of each plate, which is constant at the base (this is required for installation on the SERN). This width is 152 mm. Because of this, the deck plates were split into 152 x-coordinates spaced evenly apart, with analysis only focused on 76 while assuming symmetry of the plates. This was done because the base x-coordinates for every plate are the same, which led to a chromosome containing 76 genes. The genes themselves are the y-coordinate lengths of the deck plate, as measured in distance from the base of the plate. Here, the nominal case has a constant length of 143 mm, while the no deck case has a constant length of 53 mm. The chromosomes for these two plates are 76 instances of the value 143, and 76 instances of 53, respectively. For plates with varying shapes (most are triangles, trapezoids, or hexagons), the varied second y-coordinate was recorded with the corresponding x-coordinate location. For triangles, the tip of the triangle is simply the y-coordinate in last bit of the chromosome (the halfway point in the plate). For trapezoids and hexagons, the bits were interpolated between the two distinct y-coordinate points on the plate. These methods allow for consistent and agreeable x-coordinates with customization of the y-coordinate genes. Output chromosomes can easily be plotted and created in CAD software before manufacturing and implementation.

2) Neural Network: Due to the lengthy time with manufacturing and testing aft deck plates, it would be unrealistic to determine the fitness of every generated geometry from the GA. Rather, a simulation approach was utilized with a neural network. As explained prior, this NN predicts OASPL, which serves as the objective minimization for the GA. Neural networks consist of artificial neurons connected to each other with assigned weights and biases. Deep neural networks (DNN) expand upon an ANN by adding additional hidden layers. At each layer, a summation of the linear combinations of input variables is given by:

$$s = XW + b \tag{5}$$

With a nonlinear activation function example given as:

$$f(s) = \frac{1}{1 + e^{-s}} \tag{6}$$

For this neural network, a Rectified Linear Units, or ReLU activation function was utilized. This was done to avoid the possible vanishing gradient problem with sigmoid activations.

To train the network, a backpropagation algorithm was used. The initial weights and biases between each node are randomly generated. These values are tweaked by training the algorithm, where the experimentally determined output is compared to the initialyl generated output. This comparison calculates the error as root mean squared error. The network cycles through epochs until the error reaches a global minimum. The backpropagation are updated using the following equation:

$$w_{kj}^{i+1} = w_{kj}^{i} - \alpha \frac{\delta C}{\delta w_{kj}} \tag{7}$$

Where w_{kj} is an element of the weight matrix, C is the cost function, and α is the learning rate. The weights for this neural network were updated using gradient descent.

The inputs to the model were restricted to simple, low-dimensional geometric and flow conditions. This allows for analysis of possible contributors to noise parameters common to the nozzle design process. The feature space is shown in Fig. 13, with a summary of settings shown in 14.

1	NPR_1	7	NPR_1 - NPR_3
2	NPR_3	8	Nozzle Aspect Ratio
3	T_1	9	Symmetry
4	NTR_1	10	L_d/D_h
5	NTR_3	11	Area Percentage of Main Stream
6	No. of Streams	12	Expansion Characteristics

Fig. 13. Feature Space of Predictive Neural Network [1].

OASPL is calculated by integrating the frequency dependent sound pressure level (SPL), with the frequency non-dimensionalized by the hydraulic diameter D_h and and the jet exit velocity U_j.

$$OASPL = \int SPL(f)df \tag{8}$$

where the frequency dependent sound pressure level is given by:

$$SPL(f) = 20\log_{10}\frac{P_{\text{rms}}(f)}{P_{\text{ref}}}dB \tag{9}$$

Where P_{ref} was 20 μPa.

The neural network settings are summarized in Fig. 14.

Hidden Layers	1
Nodes	2048
Batch Size	30
Epochs	350
Activation	ReLU
Objective	Mean Squared Error
Optimizer	Adam
Learning Rate	0.01

Fig. 14. Summary of NN Features.

IV. Results

As a base for comparison, OASPL was determined for nominal conditions with a varied NPR_3. As seen in Fig. 15, all 3 conditions are within 0.5 dB of one another at the far-field angle. The peak noise emission directs consistently to 25° from the jet axis. The nominal condition exhibits a 4 dB spike in the OASPL 60° from the jet axis.

This experimental result serves as a basis of comparison to the predictive capabilities of the neural network. Out of the 300 total data cases used for the neural network (see Fig. 8), results for the 10 validation cases were plotted in a similar manner. These 10 cases featured varied operating conditions. The neural network was shown to correctly predict OASPL

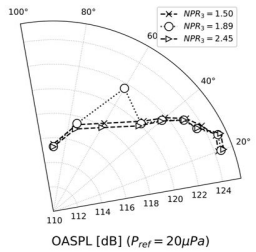

Fig. 15. OASPL Directivity [1].

to within 4 dB at its worst with most results falling within ±1dB. This also correctly predicts the direction of peak noise as well as trends in directionality. Figures 16 and 17 show the predicted results versus experimentally determined results for two cases. This clearly shows the incredible accuracy of both predicted magnitudes and directionality of the system.

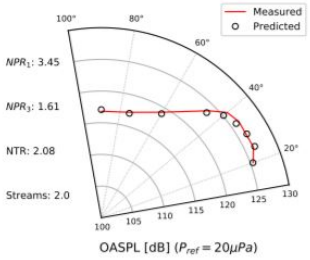

Fig. 16. OASPL Predictive Results.

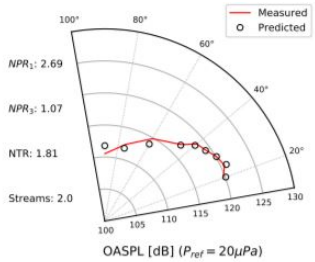

Fig. 17. OASPL Predictive Results.

This shows the results are reliable enough to serve as a rapid predictive method for OASPL. This allows the GA to accurately predict results for varied deck plate geometries and use the neural network as a model for its evaluation.

However, due to the ongoing Covid-19 Pandemic and deadlines of this project, analysis and results were altered slightly. Access to the experimental facility has been paused for the near future and prevented the ability to obtain data to train the newly formatted neural network. Many old data sets were also unobtainable due to restrictions with accessing campus computers and files. With the restrictions in place, an old NN was utilized as a predictive OASPL measure for a slightly modified GA. This was again done because new training data for the reformatted NN was unobtainable. The

shape optimization was restricted to a mean deck length to accommodate the original NN settings, which was originally trained with only 4 characteristic deck lengths. With this method, the GA consistently converges to resulting individuals featuring the maximum allowed deck length of 233 mm. The minimum predicted peak OASPL magnitude was 125.2 dB, which only varied slightly for less fit individuals and was accompanied by slightly higher average results for each trail run. The GA averages a 53 second run time. The results may be attributed to the dominant 34 kHz signature present in every case. This is likely preventing the GA from producing more fit individuals due to the inability to adjust to that signature. It is also likely impacting the NN's predictive OASPL capabilities. This instability can hopefully be eliminated in the coming months when a new splitter plate geometry is installed, which has been shown in simulations to drastically reduce the energy of the structures formed in the aft-splitter plate region.

V. Discussion

Despite the limited conditions, real progress was made on this project and has formed a solid base for continued improvement in the near future. Specifically, the neural network was modified to accommodate more specific and diverse deck plate geometric data. Although this was unable to be trained or used, it is prepared and ready once experimental training data can be obtained. A GA to work in tandem with this NN was also developed with the ideal geometric properties discussed. Again, this will be used with the new NN once training data is obtained. However, to satisfy the needs of this project, a GA was produced that optimized the mean deck length rather than the full coordinate system discussed prior. This was used in tandem with an old NN model that was able to be trained with old data. This showed a direct correlation between decreased OASPL to increased mean deck plate length. Although the results only yielded a 1-2% decrease, it agrees with prior experiments and turbulence theory. For example, see the following figure, which compares the far-field spectra for the "no deck" (53 mm) case versus the maximum length case (233 mm). The 34 kHz instability is seen in both examples, but the "no deck" case features other spikes in the acoustic spectra caused by other turbulent structures contributing to the OASPL.

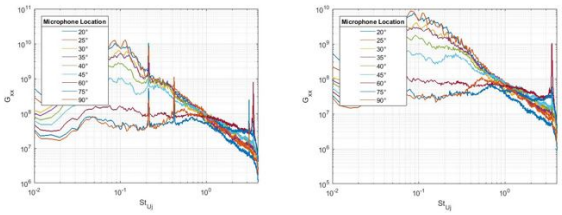

Fig. 18. Experimentally Recorded Spectra Comparison of No Deck Case (Left) vs. Maximum Deck Length Case (Right).

This also shows the domination of the far-field spectra by the 34 kHz structure. This may be preventing more accurate or achievable optimization due to the OASPL being so heavily influenced by this instability in every deck case.

Overall, this further verifies that the NN proves to be a far more efficient method for rapid predictions compared to other computational methods, such as CFD.

VI. Future and Ongoing Work

This project was again unfortunately impacted due to the COVID-19 Pandemic. This has delayed progress significantly, pushing expected progress months into the future. At the time of this paper submission, Skytop Turbulence Laboratories was recently deemed essential personnel for Syracuse University and allowed to return to work. Although delayed, this will allow for immediate continuation on the remainder of this investigation. Specifically, continuation of acquisition of experimental data for the existing deck plates will continue. This data will be used to train the NN for use with its newly adapted parameters. This will prove to be a time consuming process to replicate the last training data set but with 27 deck plates compared to the original 4. Once this is completed, the correct GA can be implemented with the NN to produce the originally desired results. These results will then be manufactured and tested to verify results.

Within the coming weeks, a new splitter plate (half thickness to the current) will be installed. Data will be recorded for this along with all of the existing deck plates. All of this data will continue to be fed to the neural network to continue training. This will require reformatting the neural network to incorporate the new splitter plate input setting. This is also expected to eliminate the characteristic 34 kHz instability dominating the OASPL values. This should drastically improve the NN and GA's abilities to analyze and optimize the reduction of energies in the lower frequency instabilities.

For the genetic algorithm, more deck plates can be produced to increase the material population size and available data. Verification on the produced results can commence to provide qualitative accuracy data.

More dimensional freedom could be added to the GA. Perhaps a width alteration could be explored on the basis of the current "infinite" width plate. This will likely delay if not prevent vortex instabilities forming in the aft corner regions of the MARS, further reducing the OASPL. This has been found to slightly reduce OASPL in previous experiments.

VII. Acknowledgments

A special thanks to the entire Skytop Turbulence Laboratories group for their help and input to this project. Specifically, a huge thanks to Dominic DiDominic, Tyler Fitzgerald, and Andrew Tenney for their prior work on similar projects and for bringing machine learning to Skytop Turbulence Labs. They inspired my interest in machine learning and encouraged me to enroll in a class focusing on it. A special thanks to Dr. Chilukuri Mohan for accepting me into his Evolutionary Algorithms course (despite not having the prerequisites!) This study was provided funding via research grants by the Air

Force Office of Scientific Research (AFOSR) grant number FA9550-19-1-0081 and Spectral Energies LLC.

REFERENCES

[1] Tenney, Andrew Steven, "Modern Methods in Machine Learning as Applied to the Study of a Complex Supersonic Jet Flow" (2019). Dissertations - ALL. 1023. https://surface.syr.edu/etd/1023

[2] Berry, Matthew, "Investigating the Interaction of a Supersonic Single Expansion Ramp Nozzle and Sonic Wall Jet" (2017). Dissertations - ALL. 819. https://surface.syr.edu/etd/819

[3] Investigating the Structures of Turbulence in a Multi-Stream, Rectangular, Supersonic Jet (2019). Dissertations - ALL. 745. https://surface.syr.edu/etd/745

[4] Valackaitė, Laisvūnė & Mačiūnas, Darius & Glėbienė, Elena. (2013). Shape Optimization of Two-dimensional Body Utilizing Genetic Algorithms.

[5] Holst, Terry & Pulliam, Thomas, "Aerodynamic Shape Optimization Using a Real-Number-Encoded Genetic Algorithm" (2001). https://ntrs.nasa.gov/archive/nasa/casi.ntrs.nasa.gov/20010003442.pdf

[6] Simmons, R. J., "Design and control of a variable geometry turbofan with and independently modulated third stream," Ph.D.thesis, The Ohio State University, 2009.

[7] Stack, C. M., Gaitonde, D. V., Agostini, L., Berry, M. G., Magstadt, A. S., and Glauser, M. N., "Numerical investigation of a supersonic multistream jet with an aft-deck," 54th AIAA Aerospace Sciences Meeting, 2016, American Institute of Aeronautics and Astronautics Inc, AIAA, 2016.

[8] Stack, C. M., and Gaitonde, D. V., "Shear Layer Dynamics in a Supersonic Rectangular Multistream Nozzle with an Aft-Deck," AIAA Journal, Vol. 56, No. 11, 2018, pp. 4348–4360.

[9] Gist, Emma D. et al, "On the Control of a Rectangular Supersonic Multi-Stream Flow Using Spanwise Geometric Modifications" AIAA Aviation 2020 Forum.

[10] Ruscher, Christopher J. et al, "Investigation of a Supersonic Jet from a Three-Stream Engine Nozzle" AIAA Journal 2018 56:4, 1554-1568. https://arc.aiaa.org/doi/abs/10.2514/1.J055910

[11] DiDominic, Dominic Christian et al,"Complex Nozzle Optimization Techniques Using Machine Learning" AIAA Scitech 2020 Forum. https://arc.aiaa.org/doi/abs/10.2514/6.2020-1866

[12] Andrew S. Tenney, Mark N. Glauser, Jacques Lewalle, and Christopher J. Ruscher. A Deep Learning Approach to Jet Noise Prediction. AIAA, 1 2018. AIAA-2018-1736.

[13] Pinqing Kan, Christopher J. Ruscher, Jacques Lewalle, and Sivaram Gogineni. Near- field shock/shear-layer interactions in a two-stream supersoinic rectangular jet from three-stream engine. AIAA Journal, 56, March 2018.

[14] Pyvolution, https://pyvolution.readthedocs.io/en/latest/Overview.html

[15] Distributed Evolutionary Algorithms in Python https://github.com/DEAP

[16] Keras Documentation https://github.com/keras-team/keras/tree/master/docs